small methods
www.small-methods.com

A Mechanochemically-Triggered, Self-Powered Flash Heating Synthesis of Phosphorous/Caron Composites for Li-Ion Batteries

Yating Yuan, Juntian Fan, Zhenzhen Yang, Shannon Mark Mahurin, Huimin Luo, Tao Wang, and Sheng Dai**

"Flash heating" that transiently generates high temperatures above 1000 °C has great potential in synthesizing new materials with unprecedently properties. Up to now, the realization of "flash heating" still relies on the external power, which requires sophisticated setups for vast energy input. In this study, a mechanochemically triggered, self-powered flash heating approach is proposed by harnessing the enthalpy from chemical reactions themselves. Through a model reaction between Mg_3N_2/carbon and P_2O_5, it is demonstrated that this self-powered flash heating is controllable and compatible with conventional devices. Benefit from the self-powered flash heating, the resulting product has a nanoporous structure with a uniform distribution of phosphorus (P) nanoparticles in carbon (C) nanobowls with strong P—C bonds. Consequently, the P/C composite demonstrates remarkable energy storage performance in lithium-ion batteries, including high capacity (1417 mAh g^{-1} at 0.2 A g^{-1}), robust cyclic stability (935 mAh g^{-1} at 2 A g^{-1} after 800 cycles, 91.6% retention), high-rate capability (739 mAh g^{-1} at 20 A g^{-1}), high loading performance (3.6 mAh cm^{-2} after 100 cycles), and full cell cyclic stability (90% retention after 100 cycles). This work broadens the flash heating concept and can potentially find application in various fields.

1. Introduction

The development of novel materials with unprecedently properties relies on skilled synthetic techniques, with temperature playing a crucial role in directing reaction pathways and influencing product properties.[1–5] The influence of temperature on materials synthesis has been routinely investigated and is becoming predictable. For example, higher temperatures during nanomaterial synthesis typically result in larger particle sizes.[6,7] However, understanding the influence of temperature change rate (heating and cooling speed), especially ultra-high change rates (≈1000 °C s^{-1}), remains lacking due to instrumental limitations. Conventional heating devices have a limited temperature change rate (typically lower than ≈20 °C s^{-1}) due to the slow heat conduction through gas, liquid, and solid mediums. The recent realization of the "flash Joule heating" technique overcomes this heating rate limitation.[8–15] This technique involves placing chemical precursors on a carbon substrate, generating rapid heating through current flow. It achieves ultra-fast heating and cooling speeds (up to 10^5 °C s^{-1}), creating intensive thermal shock and a thermal nonequilibrium environment. By using this technique, several studies have reported the synthesis of nanomaterials and uncovered the crucial role of ultra-high temperature change rate in synthesis.[16–19] For example, Hu reported that the size and phase of high-entropy-alloy nanoparticles can be well controlled by varying heating and cooling speeds.[19] Yan synthesized lattice-strained spinel ferrites as a high-performance oxygen evolution reaction (OER) catalyst by manipulating the thermal mismatch between $NiFe_2O_4$ and the carbon substrate under thermal shock to over 1000 °C.[16] James found that various carbon precursors can be converted to turbostratic graphene by Joule flash heating. Additionally, the conversion of the 2H phase of transition metal dichalcogenides to the thermodynamically metastable 1T phase was reported by the same group using Joule flash heating. These studies have demonstrated the huge potential of the flash heating effect.[17,18]

Despite the excellent performance of products, the heating source of "flash Joule heating" still relies on the external power, which requires sophisticated setups for vast energy input. Besides, Joule heating primarily heats the surface of the material, and the heat generated may not penetrate deeply into the material. This can be a limitation for applications requiring uniform heating throughout the bulk of the material. Herein, we propose a mechanochemical triggered process that can achieve a self-powered flash heating by utilizing the enthalpy from the chemical reaction itself. It is well known that enthalpy change in chemical reactions, which is caused by bond rearrangement, describes the endothermic or exothermic nature of reactions.[20,21]

Y. Yuan, J. Fan, Z. Yang, S. M. Mahurin, H. Luo, T. Wang, S. Dai
Chemical Sciences Division
Oak Ridge National Laboratory
Oak Ridge, TN 37831, USA
E-mail: wangt@ornl.gov; dais@ornl.gov

The ORCID identification number(s) for the author(s) of this article can be found under https://doi.org/10.1002/smtd.202400460

DOI: 10.1002/smtd.202400460

Depending on the chemical state of reactants, and the number and type of bonds involved, an exothermic reaction can be very intense.[22,23] In an exothermic reaction, heat is generated at the interface between reactants, which inherently come into close contact with precursors, facilitating efficient heat conduction throughout the bulk of the material. If a reaction is fast enough, meaning a large amount of heat is released within a short time frame, flash heating is achievable. Therefore, it is possible to utilize the energy from the reaction itself to realize a flash heating effect.

In this work, as a proof of concept, we report the first realization of a self-powered flash heating effect through a mechanochemically-triggered, instantaneous exothermic reaction between a Mg_3N_2/carbon composite and P_2O_5. Readily available mechanical ball milling was introduced to create activation energy to initiate the self-propagating reaction, resulting in releasing tremendous heat within only 2.4 s and achieving a remarkable internal temperature over 1000 °C, leading to a flash heating effect. Characterizations of mechanochemical flash heating synthesized P/C composite (denoted as MFH-P/C) revealed a uniform dispersion of 60 wt % P within porous carbon matrix with the presence of a strong P—C bond which could be facilitated by high temperature flash heating. These features enable MFH-P/C to overcome the long-standing cyclic failure of P based materials, which is caused by the pulverization of the electrode during the electrochemical alloying and dealloying reactions.[24–28] As a result, MFH-P/C delivered outstanding electrochemical lithium storage properties including high capacity (1417mAh g^{-1} at 0.2A g^{-1}), long term stability (935 mAh g^{-1} after 800 cycles at 2 A g^{-1}), high-rate performance (730 mAh g^{-1} at 20 A g^{-1}), high loading performance (3.6 mAh cm^{-2} after 100 cycles), and full cell cyclic stability (90% retention after 100 cycles) which outperforms a majority of reported P based materials.

2. Results and Discussion

The mechanochemical-driven flash heating synthesis was schematically illustrated in **Figure 1a**. Ball milling of an Mg_3N_2/C composite with P_2O_5 was conducted using a commercially available ball miller, with the synthesis of Mg_3N_2/C previously published.[29] The X-ray diffraction (XRD) analysis of the synthesized Mg_3N_2/C composite is displayed in Figure S1a (Supporting Information), showing a good match with the standard peaks of Mg_3N_2. The complete removal of nitrogen is verified by X-ray photoelectron spectroscopy (XPS) measurements of the N 1s peak in the g-C_3N_4 precursor and the resulting carbon from the Mg_3N_2/C composite, as shown in Figure S1b (Supporting Information). The reaction of Mg_3N_2 with P_2O_5 was proposed through equation $5/3\ Mg_3N_2 + P_2O_5 = 5\ MgO + 2\ P + 5/3\ N_2$ (gas), which exhibits a significant decrease in Gibbs free energy ($\Delta G = -814$ kJ mol^{-1} at 20 °C) and a substantial release of enthalpy ($\Delta H = -733$ kJ mol^{-1} at 20 °C), originating from the formation of thermodynamically stable Mg—O bonds and N–N triple bonds in the products. Evidence of the flash heating effect was acquired by in situ monitoring of the reaction temperature inside a custom-modified ball milling jar (Figure S2, Supporting Information) and is shown in Figure 1b,c. It was observed that the ball milling activation process lasted for ≈10 s and caused the internal temperature to slightly increase by 2 °C before spiking up to an astonishing 1030 °C within merely 2.5 s, indicating that this is an instantaneous reaction rather than a gradual one. Such a phenomenon was enabled by the extremely fast propagation of the reaction interface, suggesting that fast reaction kinetics is the key factor in achieving the flash heating effect. The fast reaction kinetics were confirmed by the XRD pattern (figure S2b, Supporting Information) of the product from ball milling Mg_3N_2/C composite with P_2O_5 for 3 min, which shows a complete conversion of the reactants to MgO and P. The rapid decrease in temperature from 1030 °C to below 200 °C within ≈3 min, followed by a gradual cooling down to 46 °C, suggests that no continuous heat release occurs during the subsequent 2 h of ball milling, confirming that the reaction is completed within a short period of time. XRD patterns (Figure 1d) of the as-synthesized and washed product after 2 h of ball milling indicate the complete elimination of the byproduct MgO after washing with acid. The P content in MFH-P/C was investigated by thermogravimetric analysis (in Figure S3, Supporting Information), suggesting that P loading reaches 60%, which is close to the stoichiometric ratio based on the reaction. Attempts to regulate the peak temperature were also made by simply adjusting the mass of reactants, with the resulting temperature trend shown in Figure 1e. A strong correlation between reactants' mass and peak temperature was observed, which is understandable considering that enthalpy is proportional to mass. These experiments verified that the proposed mechanochemical-triggered flash heating process is feasible in a controllable manner.

The morphology and structural properties of MFH-P/C were characterized. Scanning electron microscopy (SEM) and transmission electron microscopy (TEM) images in **Figure 2** reveal the stacked porous structure of MFH-P/C, which is composed of bowl-like carbon flakes with a diameter of 100–300 nm and a thickness of 30 nm. The thickness of carbon flakes in MFH-P/C is similar to that of nano-graphite derived from Mg_3N_2/C composite (Figure S4, Supporting Information). The formation of the bowl-like structure is likely induced by the mechanical shearing force during the ball milling. The porous structure could result from the simultaneous release of N_2 and flash heating during the reaction, wherein gas evolution generates void channels, and the short-time heating prevents sintering. This unique mechanism distinguishes the mechanochemical-driven flash heating process from the traditional ball milling process, in which the latter usually results in densely packed morphology.[30–32] To study the elemental distribution in MFH-P/C, Energy Dispersive Spectrometer (EDS) elemental mapping images under different scales were acquired and displayed in the Figure 2 e,f and Figure S5 (Supporting Information), revealing the highly uniform distribution of P within C throughout micrometer and nanometer scales. TEM images in Figure 2c,d further reveal the porous structure of MFH-P/C, with amorphous phosphorus particles encapsulated by crumpled and curved carbon layers. The porosity of MFH-P/C was further characterized by nitrogen adsorption, with the isotherm displayed in Figure S6 (Supporting Information). The MFH-P/C composite has a Brunauer-Emmett-Teller (BET) surface area of 30 m^2 g^{-1}, and the adsorption mainly occurs at a high relative pressure ($P/P_0 > 0.8$, Figure S6, Supporting Information), suggesting a stacked pore structure. An appropriate porosity could enhance the electrochemical performance of alloy type anode not only by providing free space to mitigate the volume

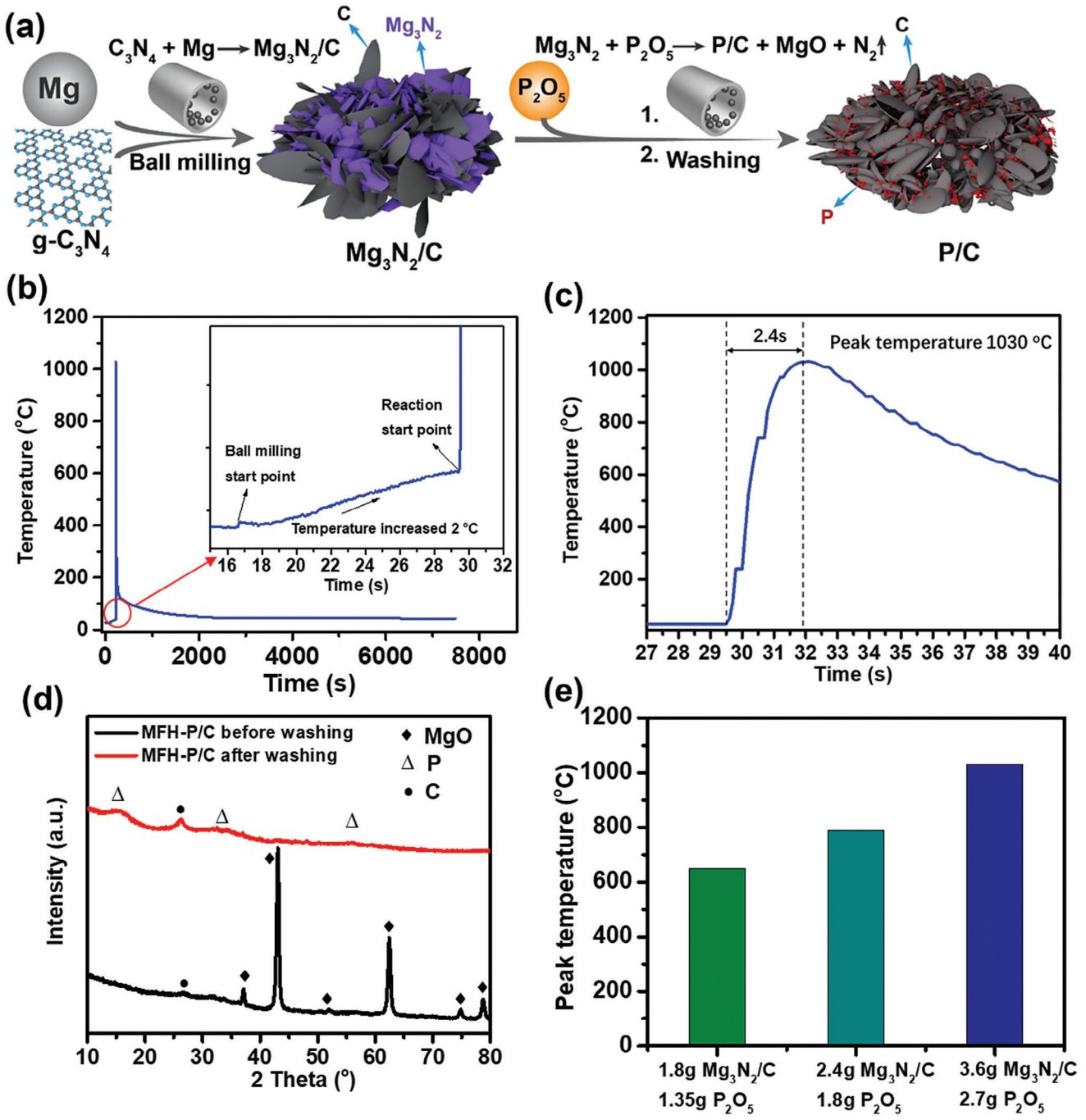

Figure 1. a) Schematic illustration of the synthesis of MFH-P/C; b) insitu measurement of temperature during the mechanochemical synthesis for 2 h, inset: the initial stage of the reaction; c)temperature profile of the first 40 s during the synthesis; d)XRD pattern of as synthesized MFH-P/C and washed MFH-P/C. e) Peak temperature recorded from different reactant mass.

change during the charging and discharging, also by the pathways for Li^+ ions transportation.[33–36] With this optimized structural features, MFH-P/C is expected to deliver superior electrochemical performance in cyclic stability and fast charging capability.

The chemical states of the samples were first investigated by Raman spectroscopy. The Raman spectrum of MFH-P/C in **Figure 3a** shows major peaks at 1348 cm^{-1} and 1610 cm^{-1}, corresponding to the D and G bands of carbon, respectively, and a weak signal ≈400 cm^{-1} from P. The I_d/I_g value, which represents the graphitization degree of carbon, was evaluated to be 1.2, much lower than the value (≈0.3 in Figure S7, Supporting Information) of the Mg_3N_2/C-derived nano-graphite, indicating a low graphitization degree of the carbon in MFH-P/C. The weakening of the

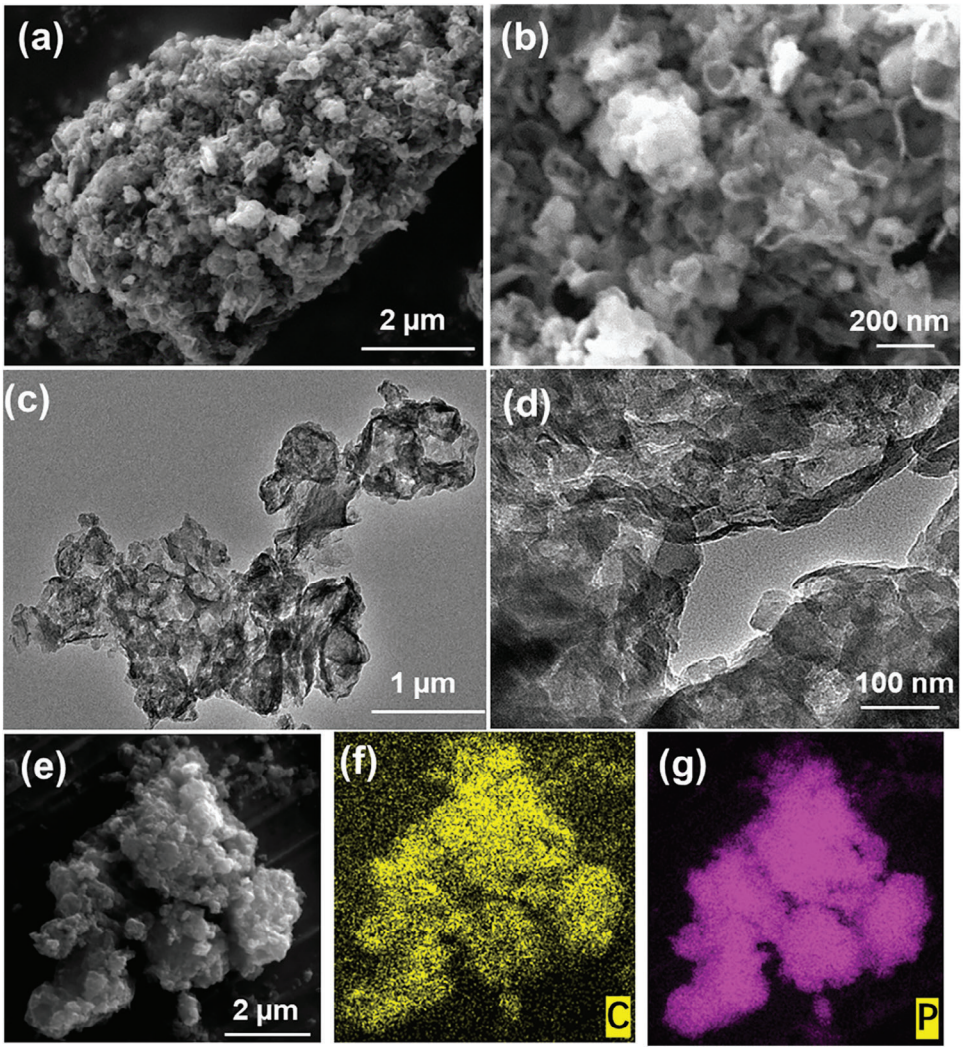

Figure 2. a, b) SEM images of MFH-P/C; c, d) TEM images of MFH-P/C; e-g) SEM-EDS element mapping of MFH-P/C.

P peaks in the Raman spectrum could result from the interaction of P with the hosts, as observed in other studies.[34,37–39]

The chemical interaction between P and C was further characterized by XPS, with the deconvoluted high-resolution P 2p spectrum of MFH-P/C comprising five peaks located at 129.6, 130.1, and 134.0 eV, assigned to 2p3/2, 2p1/2 of P—P bond and P-C, P—O bond, respectively. The P—C bond was also confirmed by deconvoluted high-resolution C 1s spectrum, displaying C═C, C—C, and P—C at 284.7, 286.2, and 288.9 eV, respectively.[30,32,40,41]The presence of P—C bonds has been reported in other P/C materials prepared through high-temperature vapor condensation or long-time ball milling.[32–41] The strong P—C bond in MFH-P/C suggests that the flash heating effect in our process may facilitate the formation of P—C bonds. The chemical bond between P and C plays a crucial role in enhancing the electrochemical performance, improving structural stability, and reducing interfacial ohmic contact in P-based materials.[30–40] The presence of oxygen in a survey in Figure 3d could originate from the exposure of the sample to air during the washing and drying process. The high-resolution O 1s spectrum in the inset of figure 3d can be deconvoluted into C—O or P—O at 533.7 eV, C═O or P═O at 532.3 eV.

The electrochemical performance was evaluated in a half coin cell configuration. **Figure** 4a shows the cyclic voltammetry (CV) curves of the MFH-P/C anode at a voltage range between 0.01 V and 3 V with a scan rate of 0.1 mV/s. A reduction wave centered at 0.5 V in the cathodic branch of the first scan can be assigned to the lithiation of P to Li_3P through multiple intermediate phases, accompanied by the formation of a solid electrolyte interface membrane.[42,43] An oxidation wave in the anodic branch centered at 1.15 V corresponds to the delithiation of Li_3P to P.[42,43] From the second to the fourth scan, the cathodic peak and anodic peak shift closer together, indicating enhanced electrochemical reversibility and implying that the MFH-P/C material undergoes an activation process during the initial cycles. Under galvanostatic charging and discharging at 0.5 A g^{-1}, the MFH-P/C electrode exhibited a charging capacity of 1296 mAh g^{-1} and a discharging capacity of 1662 mAh g^{-1} in the first cycle, resulting in a Coulombic efficiency of 78%. The irreversible capacity in the first cycle is attributed to the decomposition of electrolytes

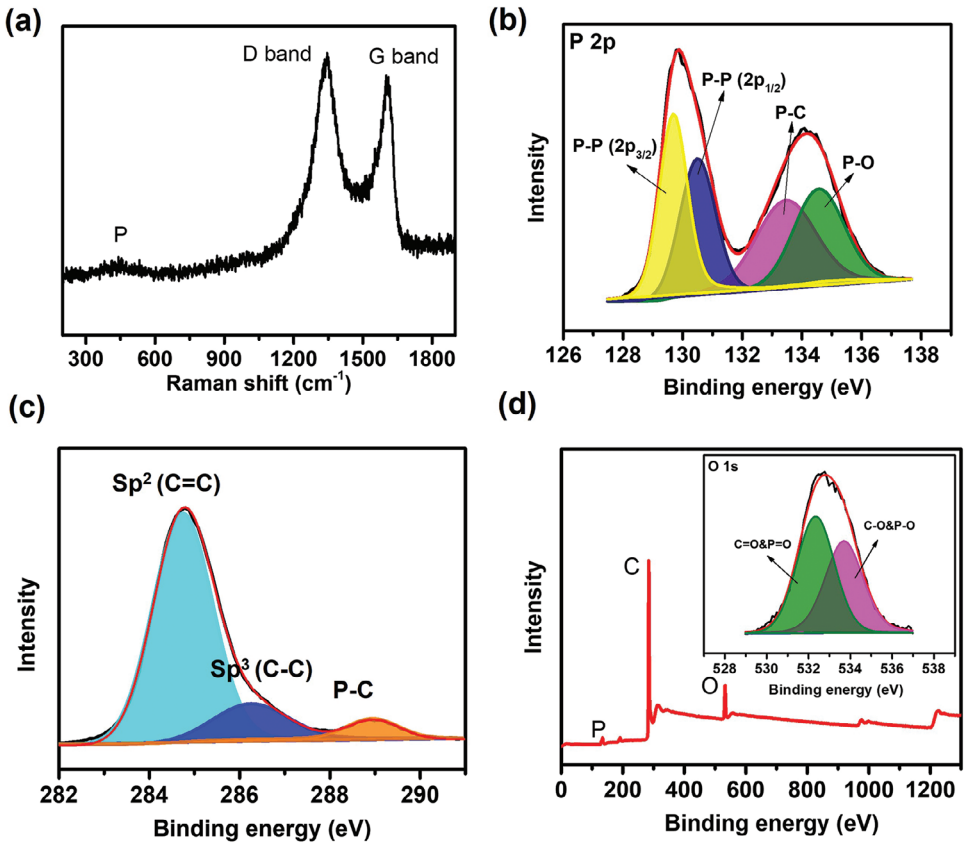

Figure 3. a) Raman spectrum of MFH-P/C; b) High resolution XPS spectrum of P 2p; c) High resolution XPS spectrum of C 1s; d) XPS survey; inset: High resolution XPS spectrum of O 1s of MFH-P/C.

and the formation of a solid electrolyte interface (SEI) layer on the electrode. After 100 cycles, the capacity of the MFH-P/C electrode was retained at 1051 mAh g^{-1}, demonstrating excellent stability. Figure 4c shows the voltage profile of the MFH-P/C anode at 0.5 A g^{-1}, with a lithiation plateau at ≈0.7 V and a delithiation plateau at ≈1.1 V, which agrees well with the CV results. The voltage profiles of the 50th cycle and 100th cycle are highly overlapped, further confirming the robust stability of the MFH-P/C electrode.

The rate performance was tested under various current densities ranging from 0.2 to 20 A g^{-1}. As shown in Figure 4e, at the current densities of 0.2, 0.5, 1, 2, 5, 8, and 10 A g^{-1}, MFH-P/C can deliver 1417, 1269, 1160, 1088, 1027, 907, and 841 mAh g^{-1}, respectively, demonstrating excellent rate performance. Even at a high current density of 20 A g^{-1}, MFH-P/C can still deliver 51.5% of the capacity at 0.2 A g^{-1}, demonstrating excellent fast charging capability. Moreover, when the current was switched back to 0.2 A g^{-1}, the capacity could recover to 1214 mAh g^{-1}, indicating a superior ability to adapt to large current variations. The voltage profiles of the MFH-P/C anode at different current densities in Figure S8 (Supporting Information) show that well-defined voltage plateaus were preserved, suggesting the alleviated polarization of the MFH-P/C anode under the high-rate test.

To evaluate the long-term cyclic performance of MFH-P/C under high current density, the electrode was tested at 2 A g^{-1} after activation at 0.5 A g^{-1} for 5 cycles. It is presented in Figure 4e that MFH-P/C exhibited remarkable cyclic stability, with a capacity of 935 mAh g^{-1} after 800 cycles, which is 91.6% of the first cycle at 2 A g^{-1} (equivalent to a capacity fading rate of 0.0011% per cycle). It is worth mentioning that the MFH-P/C electrode also exhibited a high Coulombic efficiency upon cycling. As shown in Figure S9 (Supporting Information), at 0.5 A g^{-1} the Coulombic efficiency of the MFH-P/C electrode jumped to 98.5% at the second cycle and 99.4% at the fifth cycle and maintained ≈99.6% for the rest of the cycles at 2A g^{-1}. The excellent cyclic performance and high Coulombic efficiency suggest that the drastic volume change of P particles is properly alleviated by the carbon framework, preventing the pulverization of the electrode and maintaining the integrity of the SEI layer.

To further demonstrate the potentially practical application of MFH-P/C, high loading and full cell performance were investigated. A high loading (3.125 mg cm^{-2}) electrode was tested in a half cell under the current density of 0.625 mA cm^{-2}, which shows in **Figure** 5a that an industrial level area-specific capacity of 3.6 mAh cm^{-2} can be retained after 100 cycles. The voltage profiles of the high loading electrode for the first 6, the 50th, and the 100th cycle are shown in the Figure 5b, demonstrating MFH-P/C 's capability of delivering stable and high areal capacity without producing large polarization. The increase in charge capacity during the first 5 cycles is likely due to insufficient penetration of electrolyte in the high loading electrode, which can be mitigated by a few cycles of activation. The full coin cell was assembled by

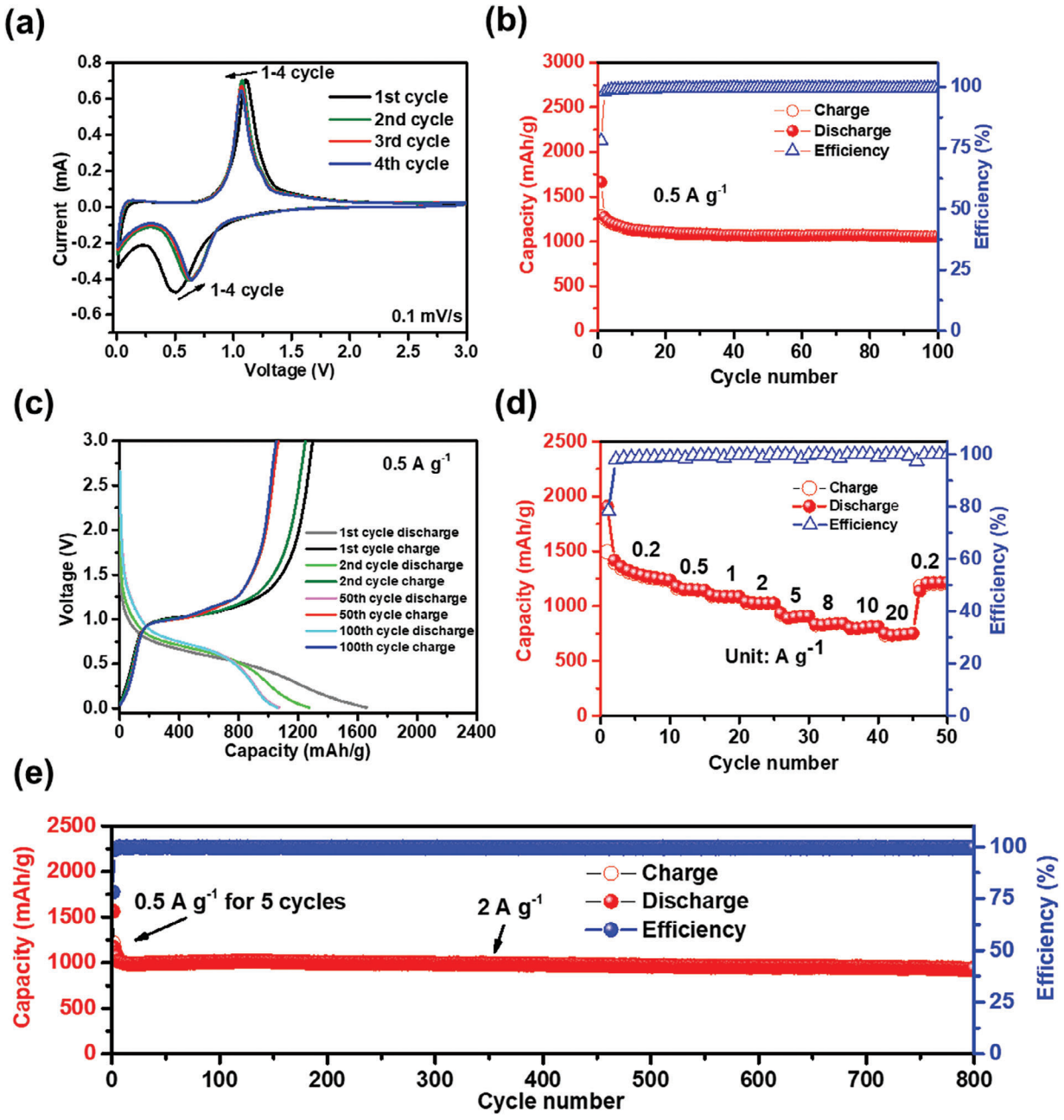

Figure 4. a) CVs of MFH-P/C anode at a scan rate of 0.1 mV s^{-1}; b) Cyclic performance of MFH-P/C anode at 0.5 A g^{-1}; c) Voltage profile of MFH-P/C anode at 0.5 A g^{-1}; d) rate performance of MFH-P/C anode; e) cyclic performance of MFH-P/C anode at 2 A g^{-1} after activation at 0.5 A g^{-1} for 5 cycles.

pairing the MFH-P/C anode with a $LiFePO_4$ cathode. The voltage profile and cyclic performance of the full cell under a high current density of 2 A g^{-1} (based on anode) are displayed in Figure 5c and Figure 5d. The full cell exhibits a well-defined discharging plateau at ≈2.3 V with a capacity of 700 mAh g^{-1} (based on anode) and a capacity retention of 90% after 100 cycles, demonstrating the potential application. The detailed comparison of the electrochemical performance of MFH-P/C with previously reported P-based materials is listed in Table S1 (Supporting Information), which further confirms the advantage of our process.

3. Conclusion

In conclusion, we have demonstrated a mechanochemical-driven self-powered flash heating process using a model reaction between an Mg_3N_2/C composite and P_2O_5 as proof of concept. By harnessing enthalpy from this instantaneous exothermic reaction, a flash heating effect can be controllably realized in a commercially available ball miller without needing a sophisticated setup. The unique features of this process result in MFH-P/C exhibiting a highly uniform distribution of chemically bonded P in a hierarchical carbon matrix with a P concentration of 60%.

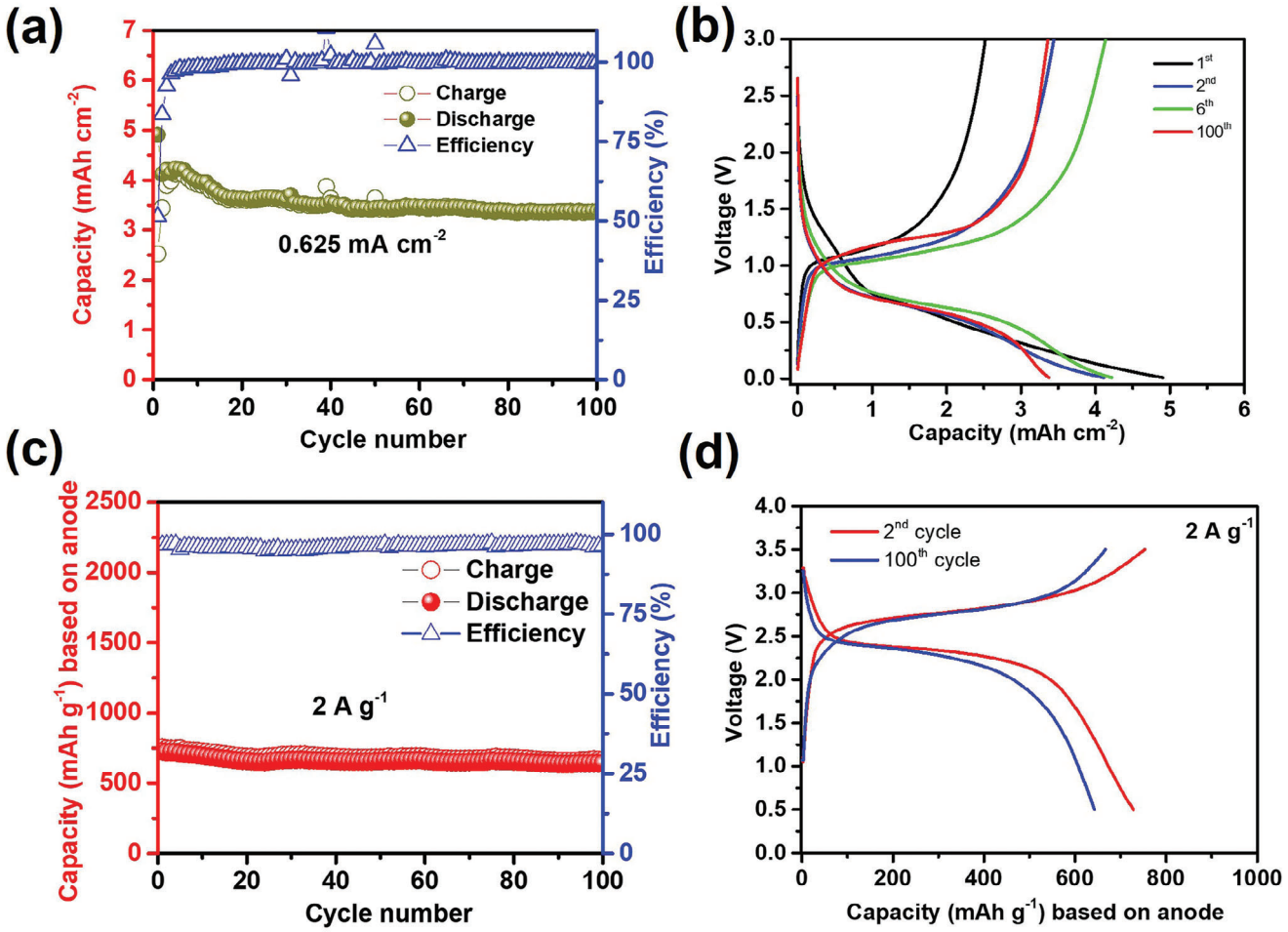

Figure 5. a) high loading performance of MFH-P/C anode under current density of 0.625 mA cm^{-2}, mass loading:3.2 mg cm^{-2}; b) Voltage profile of high loading MFH-P/C anode under current density of 0.625 mA cm^{-2}; c)cyclic performance of $LiFePO_4$|| MFH-P/C full cell at 2 A g^{-1}; d) Voltage profile of $LiFePO_4$||MFH-P/C full cell cycled at 2 A g^{-1}.

Benefiting from the advanced structure, MFH-P/C exhibits remarkable electrochemical lithium storage properties, including high capacity (1417 mAh g^{-1} at 0.2 A g^{-1}), robust cyclic stability (935 mAh g^{-1} at 2 A g^{-1} after 800 cycles, 91.6% retention), high-rate capability (739 mAh g^{-1} at 20 A g^{-1}), high loading performance (3.6 mAh cm^{-2} after 100 cycles), and full cell cyclic stability (90% retention after 100 cycles). This work broadens the flash heating concept and could potentially find application in various fields.

Supporting Information

Supporting Information is available from the Wiley Online Library or from the author.

Acknowledgements

This work was supported by the U.S. Department of Energy, Office of Science, Basic Energy Sciences, Materials Sciences and Engineering Division under contract number DEAC05-00OR22725 with the US Department of Energy (DOE).

Conflict of Interest

The authors declare no conflict of interest

Data Availability Statement

The data that support the findings of this study are available from the corresponding author upon reasonable request.

Keywords

batteries, flash heating, mechanochemistry, phosphorus

Received: March 28, 2024
Revised: August 11, 2024
Published online:

[1] C. J. Bartel, S. L. Millican, A. M. Deml, J. R. Rumptz, W. Tumas, A. W. Weimer, S. Lany, V. Stevanović, C. B. Musgrave, A. M. Holder, *Nat. Commun.* **2018**, *9*, 4168.

[2] F. Pan, K. Ni, T. Xu, H. Chen, Y. Wang, K. Gong, C. Liu, X. Li, M. L. Lin, S. Li, X. Wang, W. Yan, W. Yin, P. H. Tan, L. Sun, D. Yu, R. S. Ruoff, Y. Zhu, *Nature* **2023**, *614*, 95.
[3] I. W. M. Smith, *Chem. Soc. Rev.* **2008**, *37*, 812.
[4] D. Wang, C. Zhou, A. S. Filatov, W. Cho, F. Lagunas, M. Wang, S. Vaikuntanathan, C. Liu, R. F. Klie, D. V. Talapin, *Science* **2023**, *379*, 1242.
[5] Y. Yao, Q. Li, J. Zhang, R. Liu, L. Jiao, Y. T. Zhu, Z. Liu, *Nat. Mater.* **2007**, *6*, 283.
[6] X. C. Jiang, W. M. Chen, C. Y. Chen, S. X. Xiong, A. B. Yu, *Nanoscale Res. Lett.* **2010**, *6*, 32.
[7] D. Mott, J. Galkowski, L. Wang, J. Luo, C. J. Zhong, *Langmuir* **2007**, *23*, 5740.
[8] D. Xia, J. Mannering, P. Huang, Y. Xu, Q. Li, H. Li, Y. Qin, A. N. Kulak, R. Menzel, *J. Am. Chem. Soc.* **2024**, *146*, 159.
[9] J. H. Cha, S. H. Cho, D. H. Kim, D. Jeon, S. Park, J. W. Jung, I. D. Kim, S. Y. Choi, *Adv. Mater.* **2023**, *35*, 2305222.
[10] Z. Zhang, Y. Liu, X. Su, Z. Zhao, Z. Mo, C. Wang, Y. Zhao, Y. Chen, S. Gao, *Nano Res.* **2023**, *16*, 6632.
[11] H. Xie, K. Fu, C. Yang, Y. Yao, J. Rao, Y. Zhou, B. Liu, D. Kirsch, L. Hu, *Small Methods* **2018**, *2*, 1700371.
[12] Y. Yao, K. K. Fu, S. Zhu, J. Dai, Y. Wang, G. Pastel, Y. Chen, T. Li, C. Wang, T. Li, L. Hu, *Nano Lett.* **2016**, *16*, 7282.
[13] K. S. N. Vikrant, H. Wang, A. Jana, H. Wang, R. E. García, *NPJ Comput Mater* **2020**, *6*, 98.
[14] I. V. Okulov, I. V. Soldatov, M. F. Sarmanova, I. Kaban, T. Gemming, K. Edström, J. Eckert, *Nat. Commun.* **2015**, *6*, 7932.
[15] C. E. J. Dancer, *Mater. Res. Express* **2016**, *3*, 102001.
[16] Y. Yan, J. Lin, K. Huang, X. Zheng, L. Qiao, S. Liu, J. Cao, S. C. Jun, Y. Yamauchi, J. Qi, *J. Am. Chem. Soc.* **2023**, *145*, 24218.
[17] W. Chen, Z. Wang, K. V. Bets, D. X. Luong, M. Ren, M. G. Stanford, E. A. McHugh, W. A. Algozeeb, H. Guo, G. Gao, B. Deng, J. Chen, J. T. Li, W. T. Carsten, B. I. Yakobson, J. M. Tour, *ACS Nano* **2021**, *15*, 1282.
[18] D. X. Luong, K. V. Bets, W. A. Algozeeb, M. G. Stanford, C. Kittrell, W. Chen, R. V. Salvatierra, M. Ren, E. A. McHugh, P. A. Advincula, Z. Wang, M. Bhatt, H. Guo, V. Mancevski, R. Shahsavari, B. I. Yakobson, J. M. Tour, *Nature* **2020**, *577*, 647.
[19] Y. Yao, Z. Huang, P. Xie, S. D. Lacey, R. J. Jacob, H. Xie, F. Chen, A. Nie, T. Pu, M. Rehwoldt, D. Yu, M. R. Zachariah, C. Wang, R. Shahbazian-Yassar, J. Li, L. Hu, *Science* **2018**, *359*, 1489.
[20] P. W. Atkins, J. De Paula, *Atkins' Physical chemistry*, Oxford University Press, Oxford, **2014**.
[21] D. Keifer, *J. Chem. Educ.* **2019**, *96*, 1407.
[22] Y. H. Hu, Y. Huo, *J. Phys. Chem. A* **2011**, *115*, 11678.
[23] C. Liang, Y. Chen, M. Wu, K. Wang, W. Zhang, Y. Gan, H. Huang, J. Chen, Y. Xia, J. Zhang, S. Zheng, H. Pan, *Nat. Commun.* **2021**, *12*, 119.
[24] W. Liu, H. Zhi, X. Yu, *Energy Storage Mater.* **2019**, *16*, 290.
[25] Y. Fu, Q. Wei, G. Zhang, S. Sun, *Adv. Energy Mater.* **2018**, *8*, 1703058.
[26] Y. S. Hu, R. Demir-Cakan, M. M. Titirici, J. O. Müller, R. Schlögl, M. Antonietti, J. Maier, *Angew. Chem., Int. Ed.* **2008**, *47*, 1645.
[27] H. Jin, S. Xin, C. Chuang, W. Li, H. Wang, J. Zhu, H. Xie, T. Zhang, Y. Wan, Z. Qi, W. Yan, Y. R. Lu, T. S. Chan, X. Wu, J. B. Goodenough, H. Ji, X. Duan, *Science* **2020**, *370*, 192.
[28] Z. Li, J. Ding, D. Mitlin, *Acc. Chem. Res.* **2015**, *48*, 1657.
[29] Y. Yuan, T. Wang, H. Chen, S. M. Mahurin, H. Luo, G. M. Veith, Z. Yang, S. Dai, *Angew. Chem., Int. Ed.* **2020**, *59*, 21935.
[30] J. Song, Z. Yu, M. L. Gordin, S. Hu, R. Yi, D. Tang, T. Walter, M. Regula, D. Choi, X. Li, A. Manivannan, D. Wang, *Nano Lett.* **2014**, *14*, 6329.
[31] G. L. Xu, Z. Chen, G. M. Zhong, Y. Liu, Y. Yang, T. Ma, Y. Ren, X. Zuo, X. H. Wu, X. Zhang, K. Amine, *Nano Lett.* **2016**, *16*, 3955.
[32] X. Li, G. Chen, Z. Le, X. Li, P. Nie, X. Liu, P. Xu, H. B. Wu, Z. Liu, Y. Lu, *Nano Energy* **2019**, *59*, 464.
[33] J. Zhu, Z. Liu, W. Wang, L. Yue, W. Li, H. Zhang, L. Zhao, H. Zheng, J. Wang, Y. Li, *ACS Nano* **2021**, *15*, 1880.
[34] L. Wang, X. He, J. Li, W. Sun, J. Gao, J. Guo, C. Jiang, *Angew. Chem., Int. Ed.* **2012**, *51*, 9034.
[35] Y. Yuan, W. Xiao, Z. Wang, D. J. Fray, X. Jin, *Angew. Chem., Int. Ed.* **2018**, *57*, 15743.
[36] Y. Yang, S. Liu, X. Bian, J. Feng, Y. An, C. Yuan, *ACS Nano* **2018**, *12*, 2900.
[37] J. Xu, I. Y. Jeon, J. Ma, Y. Dou, S. J. Kim, J. M. Seo, H. Liu, S. Dou, J. B. Baek, L. Dai, *Nano Res.* **2017**, *10*, 1268.
[38] D. Wei, Y. Wu, Y. Nie, J. Duan, C. Cao, J. Wu, L. Li, Z. Chen, G. Zhang, H. Duan, *Appl. Surf. Sci.* **2020**, *529*, 147114.
[39] X. Jiao, Y. Liu, T. Li, C. Zhang, X. Xu, O. O. Kapitanova, C. He, B. Li, S. Xiong, J. Song, *ACS Appl. Mater. Interfaces* **2019**, *11*, 30858.
[40] S. Zhang, C. Liu, H. Wang, H. Wang, J. Sun, Y. Zhang, X. Han, Y. Cao, S. Liu, J. Sun, *ACS Nano* **2021**, *15*, 3365.
[41] B. Liu, Q. Zhang, L. Li, Z. Jin, C. Wang, L. Zhang, Z. M. Su, *ACS Nano* **2019**, *13*, 13513.
[42] S. C. Jung, Y. K. Han, *J. Phys. Chem. C* **2015**, *119*, 12130.
[43] C. Peng, H. Chen, G. Zhong, W. Tang, Y. Xiang, X. Liu, J. Yang, C. Lu, Y. Yang, *Nano Energy* **2019**, *58*, 560.